Research Square

Preprints are preliminary reports that have not undergone peer review. They should not be considered conclusive, used to inform clinical practice, or referenced by the media as validated information.

Production of natural uranium chemical concentrate by sorption-free processing of uranium solutions

Yerkebulan Sadykov
Satbayev University
Tatyana Chepushtanova
Satbayev University
Ata Akcil
ata.akcil@nu.edu.kz

Nazarbayev University
Armanbek Omirgali
Satbayev University
Manarbek Kylyshkanov
Satbayev University
Mariya Kopbayeva
Satbayev University

Article

Keywords: uranium, filtration mother liquors, ultrafiltration, fine-dispersed phase, colloidal particles, loss diagnostics, concentration, scanning electron microscopy, energy-dispersive X-ray microanalysis

Posted Date: September 18th, 2026

DOI: https://doi.org/10.21203/rs.3.rs-10850359/v1

License: This work is licensed under a Creative Commons Attribution 4.0 International License. Read Full License

Additional Declarations: No competing interests reported.

Production of natural uranium chemical concentrate by sorption-free processing of uranium solutions

Yerkebulan Sadykov[a], Tatyana Chepushtanova[a], Ata Akcil[b,*], Armanbek Omirgali[a], Manarbek Kylyshkanov[a], Mariya Kopbayeva[a]

[a]*Satbayev University, Metallurgical process, Heat engineering and Technology of Special Materials Department, Almaty, Republic of Kazakhstan*

[b]*School of Mining and Geosciences (SMG), Nazarbayev University, 6 Block, 53 Kabanbay Batyr Avenue, 010000 Astana, Republic of Kazakhstan*

Abstract

The present study examines the applicability of ultrafiltration in the processing of filtration mother liquors generated during uranium production. In contrast to the conventional approach, in which membrane treatment is considered primarily as a method for solution clarification and purification, the present work demonstrates that ultrafiltration can additionally serve as a promising diagnostic tool for process monitoring. It is shown that the application of ultrafiltration makes it possible to detect the presence of fine-dispersed uranium-bearing phases, concentrate them within a small volume, perform subsequent identification of precipitate composition, and evaluate the magnitude of hidden uranium losses associated with mother liquors. Experimental data indicate that a significant portion of uranium may be present not only in dissolved form but also in the form of dispersed, colloidal, or mineral particle-associated compounds, which are not completely retained by conventional filtering materials. The application of ultrafiltration provides physical separation of such particles without the introduction of additional precipitating agents, thereby preserving the original nature of the isolated phase and improving the reliability of subsequent analysis. The obtained concentrate can be investigated by means of scanning electron microscopy and energy-dispersive X-ray microanalysis in order to determine particle morphology, elemental composition, and the association of uranium with iron, silicon, aluminum, calcium, and other components. The proposed approach allows ultrafiltration to be regarded as an integrated method for the diagnosis and minimization of uranium losses rather than solely as a stage of liquid-phase purification.

Keywords: uranium, filtration mother liquors, ultrafiltration, fine-dispersed phase, colloidal particles, loss diagnostics, concentration, scanning electron microscopy, energy-dispersive X-ray microanalysis.

*Corresponding author: ata.akcil@nu.edu.kz; ataakcil1@gmail.com

1. Introduction

Hydrometallurgical processing of uranium-bearing solutions comprises a series of sequentially interconnected operations aimed at the recovery, concentration, and production of commercial uranium compounds. At the final stages of processing, particular importance is attached to the completeness of separation of uranium-bearing precipitates from the liquid phase. Even under stable operating conditions of the principal hydrometallurgical processing stages, a portion of the target component may be transferred into filtration mother liquors in the form of fine-dispersed and colloidal particles. Such losses are more difficult to detect by conventional monitoring of dissolved uranium species, since they are associated not only with the chemical composition of the solution but also with the dispersed state of the solid phase.

In classical approaches to uranium ore processing, primary attention is devoted to the recovery of dissolved uranyl sulfate complexes and the subsequent precipitation of the commercial product [1]. At the same time, modern requirements for process efficiency necessitate consideration not only of dissolved uranium but also of mechanically entrained, colloidal, and sorbed uranium [2]. International guidelines on uranium recovery technologies emphasize the importance of material balance calculations, loss control, and optimization of solid-liquid separation operations [3, 4].

The most problematic losses are associated with the presence of uranium-bearing particles within the ultradisperse range. [5, 6] Such particles may be formed during peroxide precipitation, as a result of precipitate aggregate destruction, wear of filtering materials, or incomplete growth of crystalline and amorphous phases. Consequently, a portion of uranium becomes associated with particles that either pass through conventional filtering media or are retained inconsistently, thereby resulting in the transfer of uranium into the filtration mother liquors.

In this regard, ultrafiltration acquires particular importance not only as a means of solution clarification but also as a tool for process diagnostics. [7, 8] Its diagnostic function consists in the sequential implementation of four principal tasks: detection of fine-dispersed uranium-bearing impurities, their concentration within a small volume, subsequent identification of phase and elemental composition, and quantitative evaluation of hidden uranium losses. It is precisely this integrated application of ultrafiltration that constitutes the central concept of the present study.

Unlike reagent precipitation, ultrafiltration does not require the introduction of additional chemical precipitating agents and does not alter the nature of the retained particles. [9-11] This feature is of fundamental importance for diagnostic purposes, since the addition of reagents may modify the composition of the precipitate, induce coprecipitation of accompanying components, and distort the

understanding of the actual causes of uranium carryover. Membrane separation makes it possible to isolate a concentrate of the fine-dispersed phase in its original or near-original state and subsequently utilize it for microstructural and elemental analyses. [12]

The data obtained in the present study demonstrate that the ultrafiltration concentrate may contain a significant proportion of uranium associated with the solid phase. According to the material balance calculations, the precipitate isolated by ultrafiltration contained 39.2 percent uranium, corresponding to 33.6 percent of the uranium introduced into the process. A total of 60.5 percent of uranium passed into the filtrate, whereas approximately 6 percent of uranium was retained within the membrane pores and subsequently recovered during membrane regeneration. These results indicate that ultrafiltration is capable not only of separating the dispersed phase but also of identifying the proportion of uranium that, under conventional process conditions, would otherwise be regarded as unexplained technological losses.

An additional advantage of the proposed approach is the possibility of subsequent investigation of the isolated precipitates by means of scanning electron microscopy and energy-dispersive X-ray microanalysis. Such analysis enables determination of particle morphology, size distribution, and elemental composition. In the investigated precipitates, coarse, medium, and fine fractions were identified. These fractions contained sorbent fragments, iron-containing compounds, particles enriched in uranium, as well as silicon-bearing and sulfate components. Consequently, ultrafiltration in this case additionally performs the function of sample preparation for the subsequent identification of the nature of uranium-bearing carryover.

In international studies, membrane technologies are applied primarily for the retention of dissolved or complex uranium species in natural, saline, and wastewater systems. In particular, the applicability of ultra- and nanofiltration membranes for uranium retention and concentration in aqueous systems of different salinities has been demonstrated [13-15] In a number of studies, membrane processes are regarded as a promising approach for the treatment of radioactive wastewater and the removal of uranium from aqueous media. [16, 17] However, the problem addressed in the present work differs fundamentally, since ultrafiltration is employed not merely for uranium removal from solutions but for diagnosing the causes of uranium losses within a specific process stream of uranium production.

Thus, the scientific novelty of the proposed approach lies in shifting the emphasis from the purification function of ultrafiltration toward its diagnostic role. The method makes it possible simultaneously to separate the fine-dispersed phase, concentrate it, obtain material for subsequent identification, and determine the contribution of dispersed carryover to the overall uranium loss balance.

Such an approach may be utilized for refinement of material balance calculations, assessment of filtration equipment performance, identification of the causes of uranium transfer into mother liquors, and development of measures aimed at returning uranium-bearing phases to the process cycle.

The practical significance of the present work is determined by the possibility of applying ultrafiltration as a tool for operational control and process optimization. Isolation and analysis of concentrates obtained from filtration mother liquors make it possible to determine the proportion of uranium associated with mechanically entrained or colloidal forms, evaluate the potential recovery of the target component, and substantiate modifications of precipitation, filtration, or membrane regeneration conditions. This is particularly important in the processing of low-concentration streams, where even relatively small hidden losses may acquire substantial economic significance owing to the large volumes of solutions involved.

2. Materials and methods

In order to determine the uranium content and to carry out further experimental work, samples of process solutions were taken from an operating uranium mining enterprise. The process flow diagram and the sampling points are shown in Figure 1. Samples were taken from the following process stages: Sample 1 – sorption mother liquor solution (MLS); Sample 2 – filtration mother liquor solution; Sample 3 – solution from the upper part of the sludge settling tank; Sample 3-1 – homogenized solution of the sludge settling tank;

The chemical composition of the process solutions is presented in Table 1.

In accordance with the results obtained, since the highest uranium content was determined in the filtration mother liquors, further ultrafiltration separation experiments were carried out using this type of solution.

To study the morphology of the precipitates formed during solution concentration, as well as to determine their elemental composition, scanning electron microscopy was used. The studies were performed using a JSM-6510 scanning electron microscope (JEOL) equipped with an energy-dispersive accessory for X-ray spectral microanalysis, providing qualitative and quantitative analysis of the composition of the substance.

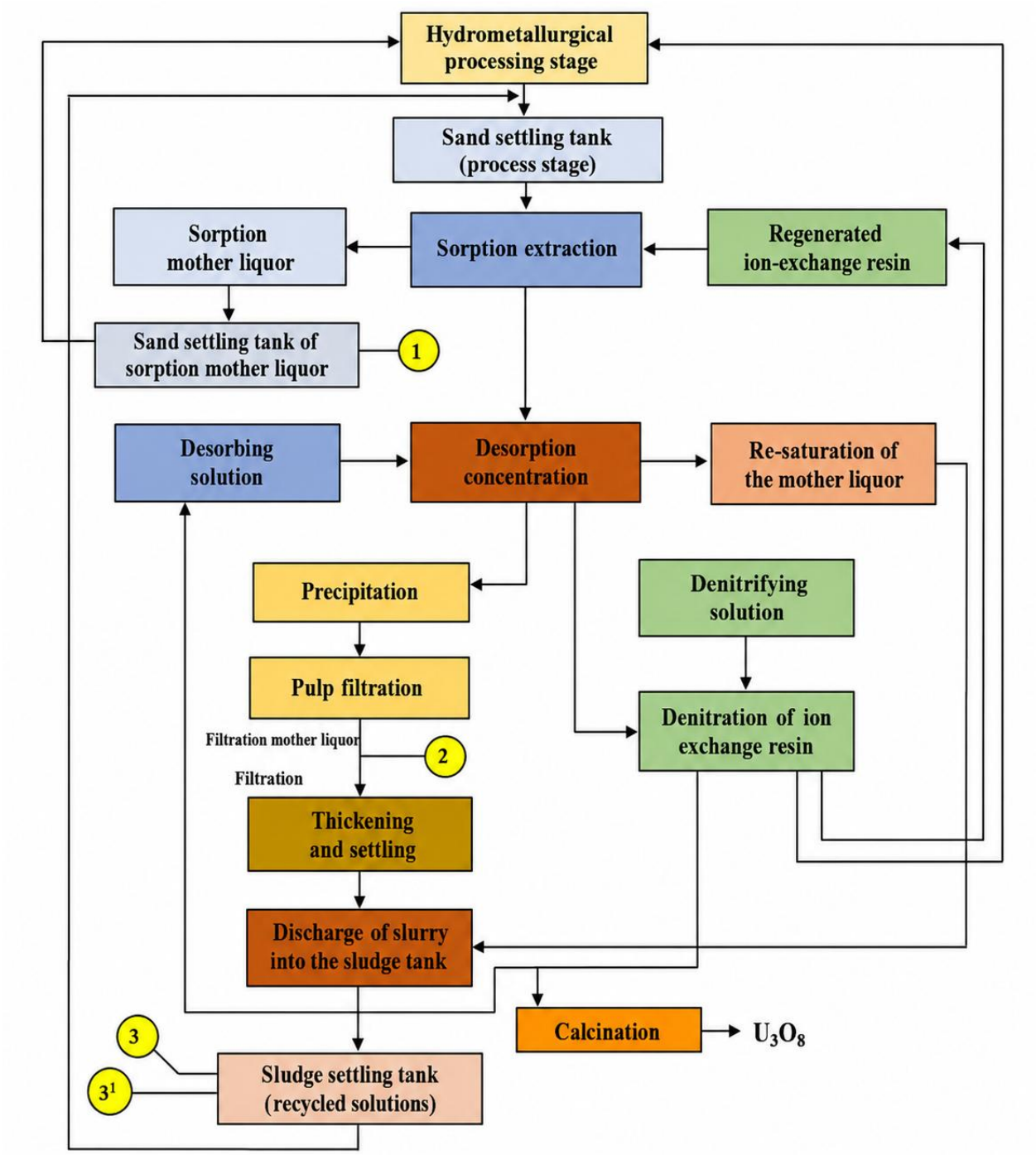

Figure 1 – Process flow diagram of the mine with sampling points:

1 – sample of sorption mother liquor (MS); 2 – sample of filtration mother liquor (MF); 3 – sample from the upper part of the recycled solution from the sludge settling tank; 3 [1] – composite sample of the recycled solution from the sludge settling tank.

Table 1 – Chemical composition of solutions, g/L.

Designation	U	Si	Fe	Al	Na	K	Mg	SO_4
Sorption mother liquor from the sand settler:	0,005	0,14	1,17	0,5	1,87	0,138	0,58	13,2

Recycled solution from sludge settling tank-1:	1,3	0,067	0,65	0,15	0,85	0,052	0,078	22,6
Recycled solution from sludge settling tank-2 (surface):	0,82	0,092	0,59	0,34	3,6	0,084	0,28	19,6
Filtration mother liquor:	0,035	0,055	0,011	0,009	10,6	0,005	0,026	11,6

For the experiments, a laboratory membrane unit manufactured by Westfalia Separator Membraflow GmbH was used, designed to assess the feasibility of concentrating fine-dispersed particles or suspensions (particle size less than 1 μm) present in low concentrations in the solution (Figures 69, 70), along with ceramic filters of the same manufacturer with a membrane area of 55 cm^2, consisting of a single channel 0.25 m in length, the body of which is made of alpha-aluminum oxide with a zirconium dioxide membrane applied to the inner surface. The equipment makes it possible to obtain highly purified solutions with the accumulation of fine-dispersed impurities in the concentrate. Two modules of the filtration unit can operate simultaneously with membranes having different pore sizes. Membranes with pore sizes of 10, 20, and 50 nm were used, with membrane regeneration after completion of the filtration process carried out using a 1 percent HNO_3 solution.

Figure 2 – General view of the laboratory membrane unit.

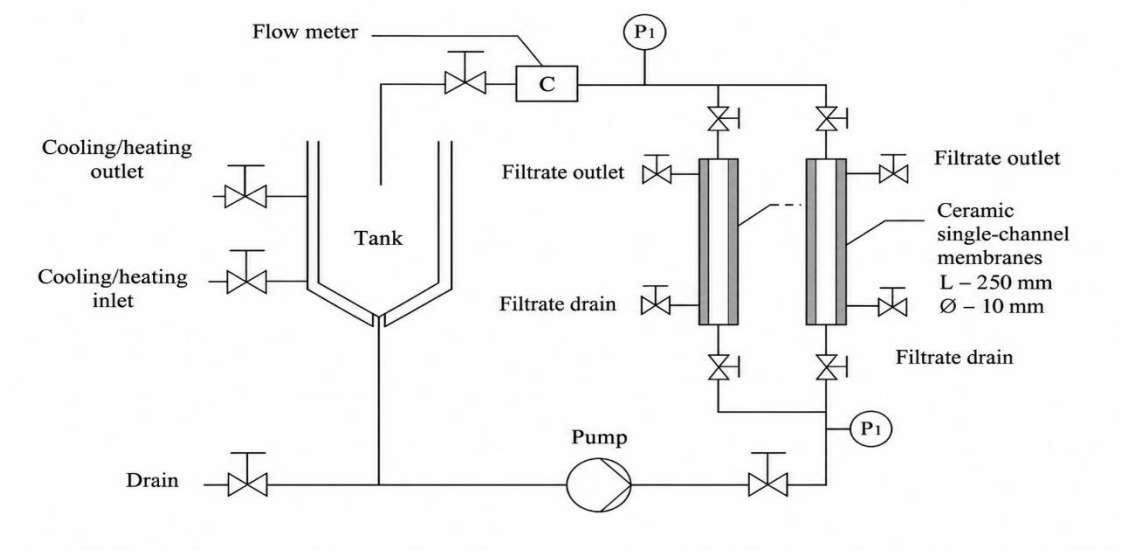

Figure 3 – Schematic diagram of the laboratory membrane unit.

The laboratory membrane unit comprises:

- a supporting frame made of stainless steel, with overall dimensions of 600 × 450 × 850 mm;

- *a feed solution tank with a volume of 15 dm³, equipped with a jacket for cooling or heating the solutions;*
- *two filtration modules;*
- *pressure gauges for monitoring pressure at the inlet to and outlet from the modules;*
- *a pipeline system for solution feed and discharge;*
- *a circulation centrifugal pump ensuring liquid circulation through single-channel ceramic filters, with a capacity of 2 m³/h at a pressure of 4 bar;*
- *an electromagnetic flow meter for measuring flow rate (flow velocity within the ceramic membrane channel) in the concentrate pipeline and for evaluating the degree of solution concentration.*

For the investigation of ultrafiltration products of recycled solutions, the following measurements were carried out:

- measurement of the optical density of filtrate solutions in order to evaluate the efficiency of the ultrafiltration process using different membrane single channels (with different pore diameters), employing a KFK-2 photoelectric colorimeter relative to a solution obtained after filtration of the initial solution (raffinate) in a cuvette with an optical path length of 50 mm using a 670 nm optical filter. Filtration of the initial solution was performed through two “blue ribbon” paper filters. The degree of clarification of the solution was calculated as the ratio of the optical densities of the filtrate and the initial unfiltered solution, expressed as a percentage;

- determination of the mass concentration of solid particles in the concentrate solution. Prior to the analysis, the mass of the “blue ribbon” paper filter was determined: the clean filter was dried in a drying oven to constant weight and weighed using laboratory balances.

An aliquot portion of the initial solution with a volume of 1000 cm³ was gradually filtered through the “blue ribbon” filter using a Büchner funnel and a Büchner flask. The residue retained on the filter was washed with 20 cm³ of distilled water. The filter with the residue was dried in a drying oven to constant weight, weighed using laboratory balances, and the mass concentration of solid particles was calculated;

- determination of the mass concentration of uranium in concentrate solutions and the mass fraction of uranium in insoluble residues. The mass fraction of uranium was determined in accordance with Measurement Procedure MVI 0306 341-2010 “Uranium. Ferro-phosphate method of determination.”

3. Results and discussion

3.1 Physicochemical characterization

Prior to conducting the investigations, the physicochemical characteristics of the filtration mother liquor solution were determined. The obtained data are presented in Table 2.

Table 2 – Physicochemical characteristics of the filtration mother liquor

Concentration, g/L;								pH	$D_{опт}$, %
U	Si	Fe	Al	Na	K	Mg	$C_{тв.ч.}$		
0,035	0,055	0,011	0,009	10,6	0,005	0,026	0,2	4,5	0,483

As can be seen from the table, the uranium concentration in the mother liquor is 0.035 g/L, the mass concentration of solid particles is 0.2 g/L, and the optical density of the solution is 0.483%.

At the first stage, filtration of the mother liquors on the laboratory unit was carried out through a membrane with a pore size of 10 nm. During filtration through the 10 nm membrane, a low filtration rate was observed. As a result, 3 liters of mother liquor were filtered, after which the filtrate flow ceased. The specific membrane productivity was 35 L/m²·h.

Increasing the pore size of the filtering membrane to 20 nm enabled filtration of the mother liquor without membrane fouling.

The volumetric flow rate of the solution through the module was 16 L/min, and the operating pressure during filtration was maintained at 2.5 bar.

The specific productivity of the 20 nm membrane was 150 L/m²·h. The overall degree of solution concentration was 16.

The results of filtration of the mother liquors on the laboratory unit are presented in Table 3.

According to the data in the table, the clarification efficiency of the solution reached 98.96 percent. The optical density of the concentrate is significantly higher compared to that of the filtrate. In the concentrate, this value was 2.712 percent, whereas in the filtrate it was 0.005 percent.

The mass concentration of solid particles in the concentrate is 4 times higher than that in the initial mother liquor solution of precipitation.

In the filtrate, as compared with the initial solution, the content of solid particles decreased by a factor of 20.

During the filtration process, a filtrate with a lower uranium content was obtained; the uranium concentration in the combined filtrate was 0.023 g/L. The degree of purification of the initial solution from uranium during filtration was 34.3 percent.

Table 3 – Results of ultrafiltration of the filtration mother liquor.

Designation of solution	**Designation of solution**		
	Uranium concentration, g/L;	Optical density of solution, percent	Concentration of solid particles in solution, g/L
Initial solution:	0,035	0,483	0,2
Filtrate			
Cycle 1	0,021	0,008	0,01
Cycle 2	0,024	0,007	0,01
Cycle 3	0,021	0,005	0,01
Cycle 4	0,040	0,006	0,01
Cycle 5	0,032	0,005	0,01
Combined filtrate:	**0,023**	**0,005**	**0,01**
Concentrate			
Cycle 1	0,09	2,058	0,5
Cycle 2	0,11	2,352	0,5
Cycle 3	0,25	2,583	0,6
Cycle 4	0,28	2,853	0,7
Cycle 5	0,33	2,889	0,8
Combined concentrate	**0,22**	**2,712**	**0,8**
Clarification efficiency of the solution, percent	98,96		

In the concentrate, the mass concentration of uranium increased by more than 6 times. The variation of optical density and the concentration of solid particles in the filtration products is shown in the graphs in Figures 4 and 5.

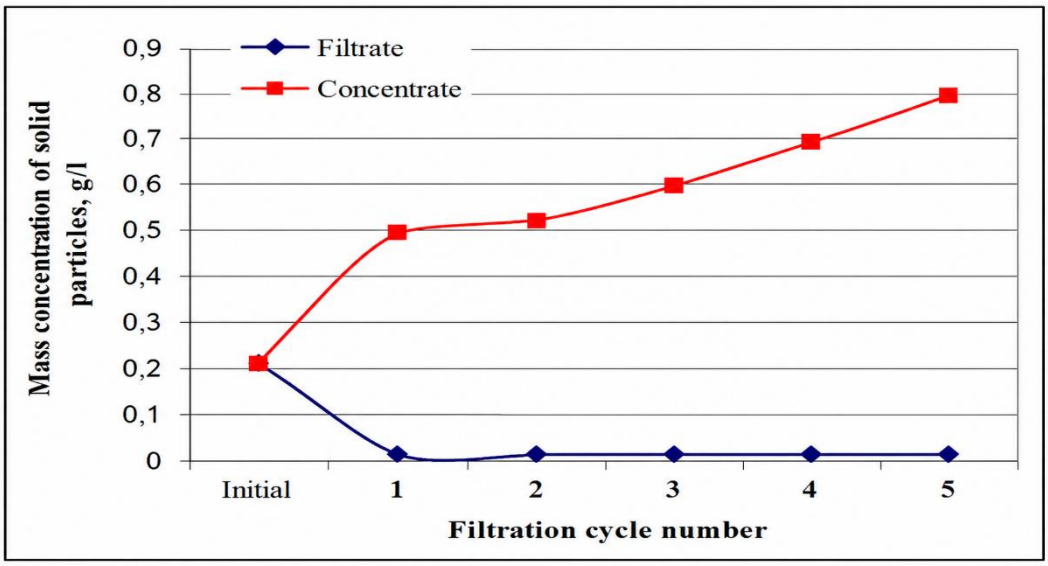

Figure 4 – Variation of the mass concentration of solid particles in the filtrate and the concentrate.

As can be seen from Figure 4, after filtration of the first portion of the precipitation mother liquor, the concentration of solid particles in the filtrate decreases from 0.2 g/L to 0.01 g/L and remains at this level until the end of the filtration process. In the concentrate, a gradual accumulation of insoluble particles occurs.

In the case of filtration of the filtration mother liquor, an additional filtering layer of precipitate is formed on the membrane surface from particles of different morphology and size, which positively affects the degree of solution purification. [18] This is also confirmed by the value of the clarification efficiency, which in the present experiment is higher (98.96 percent) compared with the previously presented data (93.7 %; 75 %).

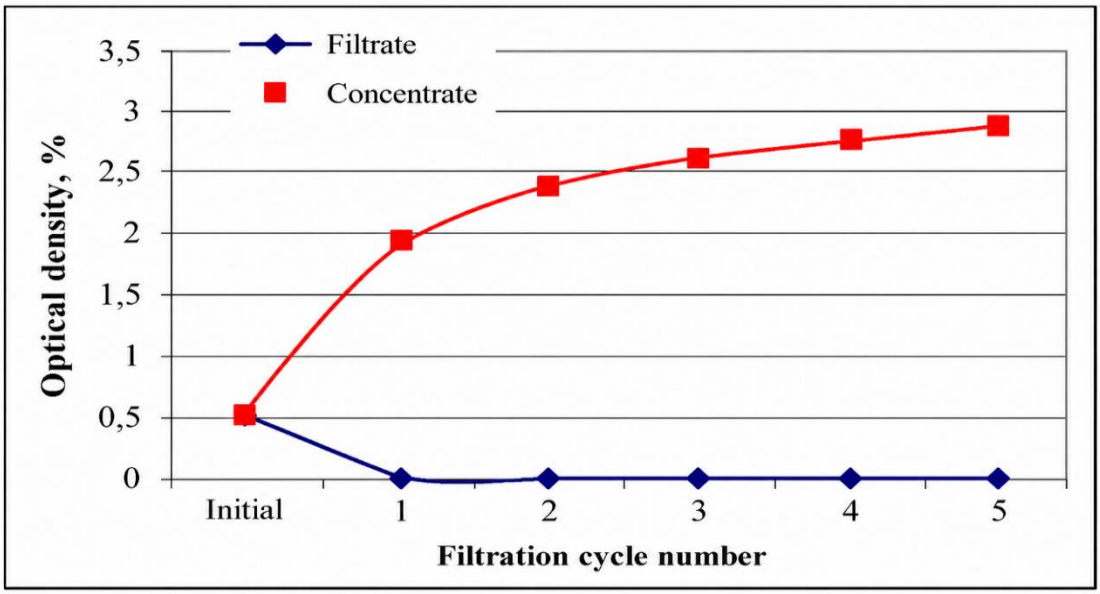

Figure 5 – Variation of the optical density of the filtrate and the concentrate over time

During the first cycle, the optical density of the filtrate reached its minimum value (Figure 5) and subsequently remained unchanged throughout the filtration process. The optical density of the concentrate increased with each cycle in accordance with the increase in the concentration of solid particles.

An insoluble precipitate was isolated from the concentrate obtained during filtration. The mass of the precipitate after filtration of the filtration mother liquor following peroxide precipitation was 0.60 g.

After separation from the solution, the precipitate was analyzed for uranium and impurity content. The analysis showed that the insoluble precipitate contained: uranium – 39.2 percent, silicon – 5.2 percent, iron – 13 percent, aluminum – 1.2 percent, magnesium – 0.1 percent, calcium – 0.32 percent.

Based on the analytical results, the uranium material balance during filtration and the distribution of uranium between the filtration products were calculated (Table 4).

Table 4 – Uranium material balance during filtration

Feed				Products						
Designation	U, g/L	V, L	$M_{U,}$ g	Designation	U, g/L	U, %	V, L	M, g	$M_{U,}$ g	**ε, %**
Mother liquor	0,035	20	0,70	**Filtrate**	0,023		18,41		0,423	**60,5**
				Precipitate		39,2		0,60	0,235	**33,6**
Membrane regeneration										
Wash solution		5,0		**Filtrate**	0,008		5,0		0,041	**5,9**
Total: 0,70g					**Total: 0,73g**					

The calculations show that the obtained precipitate contains 39.2 percent uranium, which corresponds to 33.6 percent of the uranium introduced into the process. A total of 60.5 percent of uranium passes into the filtrate from the initial solution. Approximately 6 percent of uranium is retained in the pores of the membrane and is recovered during membrane regeneration.

3.2 Investigation of filtration mother liquor precipitates by scanning electron microscopy and energy-dispersive X-ray microanalysis

During the preparation of precipitates isolated from the filtration mother liquor concentrate for analysis by scanning electron microscopy and energy-dispersive X-ray microanalysis, three conditional fractions were distinguished. Figure 6 shows the most representative fractions of the precipitates: a coarse fraction represented by fragments of sorbents, insoluble oxides, and iron sulfate complexes with particle sizes in the range of 50 to 300 micrometers; and a medium fraction

also represented by iron sulfate complexes and uranium peroxide, identified therein by energy-dispersive X-ray microanalysis.

In the coarse fraction, as shown in Figure 6(a), numerous fragments of white fibers with sizes ranging from 100 to 500 micrometers were observed, which are most likely microfragments of the filter press cloth degraded during filtration of the uranium peroxide pulp. These fibers were also observed in other fractions of the precipitate; however, during sample preparation for scanning electron microscopy (washing), they were removed, since, being an organic and readily combustible material, they could contaminate the vacuum system of the electron microscope.

Scanning electron microscopy studies established that the medium fraction, constituting not less than 83 percent of the total precipitate obtained during ultrafiltration, can be further conditionally divided into two subfractions: a coarser subfraction of particles settling onto the substrate within 40 minutes, consisting of particles with sizes in the range of 30 to 50 micrometers (medium fraction 1), and a finer subfraction settling within 2 hours, consisting of particles with sizes in the range of 2 to 20 micrometers (medium fraction 2). In addition, a fine fraction of particles settling onto the substrate within 24 hours was isolated from the concentrate, consisting of particles with sizes ranging from 0.1 to 2 micrometers, with this fraction accounting for not less than 15 percent of the total precipitate volume (Figure 7).

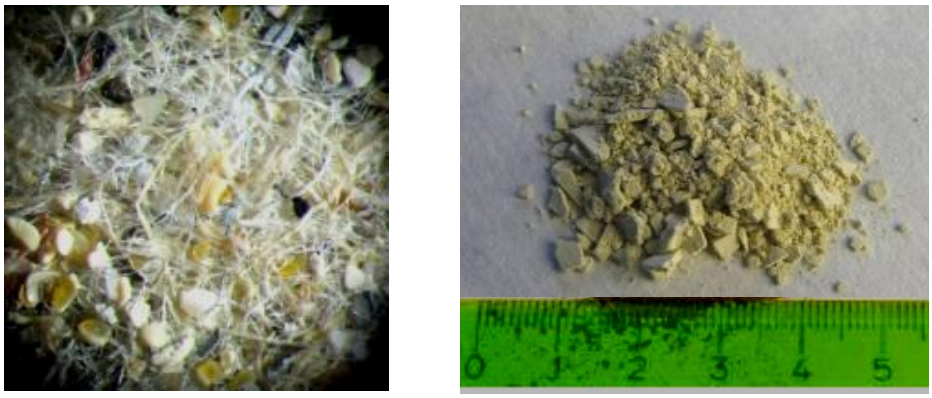

a. b.

Figure 6 – Insoluble precipitates isolated from the concentrate of the filtration mother liquor: (a) coarse fraction precipitates; (b) medium fraction precipitates.

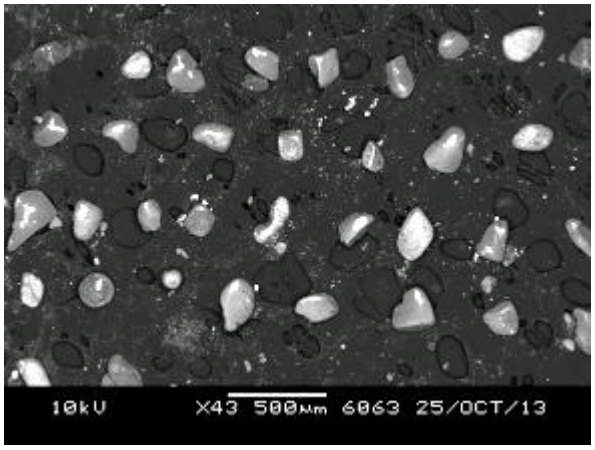

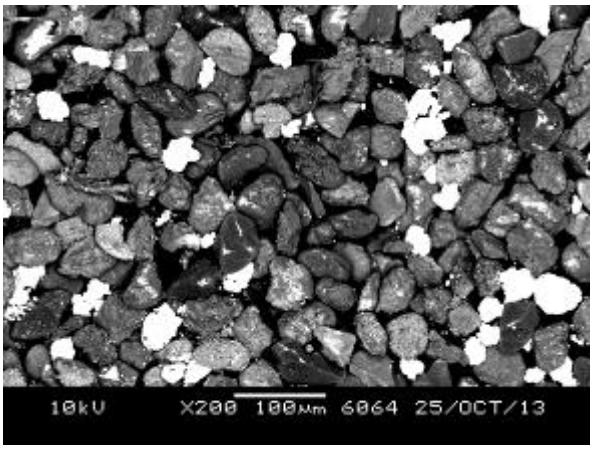

a. b.

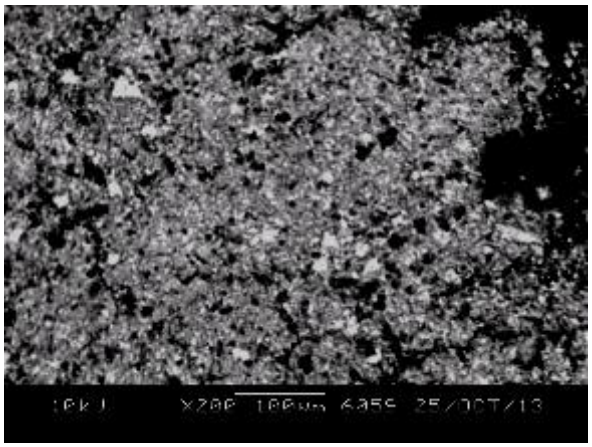

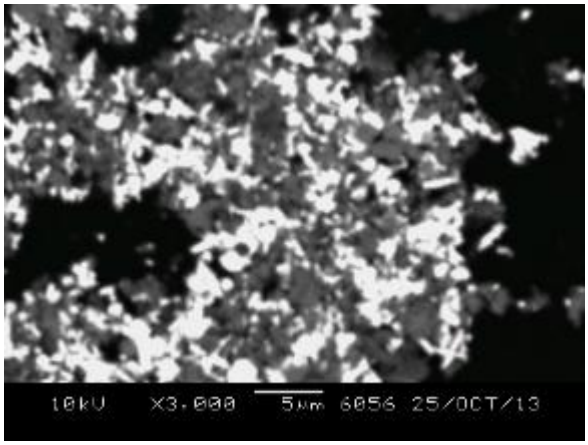

c. d.

Figure 7 – Morphology of particles of different precipitate fractions isolated from the filtration mother liquor concentrate:
(a) particles of the coarse fraction; (b) particles of medium fraction 1;
(c) particles of medium fraction 2; (d) particles of the fine fraction.

a.

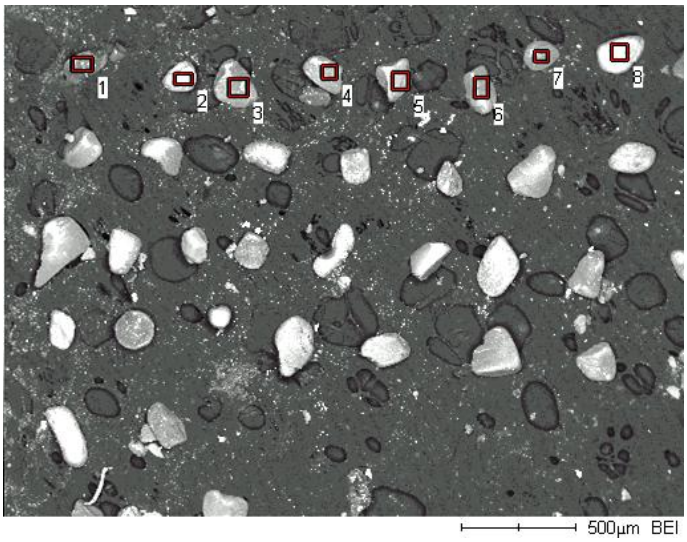

b.

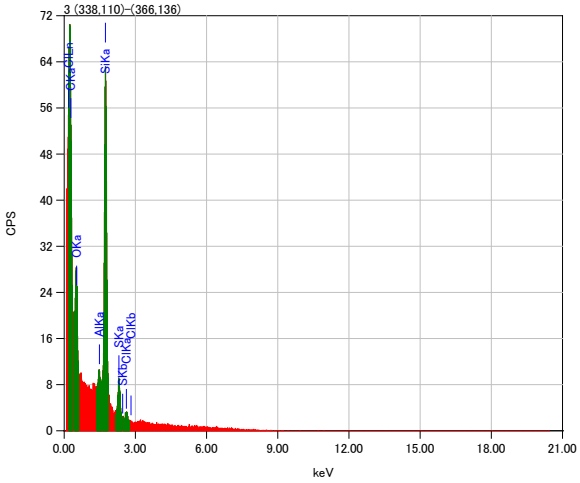

Element	mass%	Error%	At%	K
C	30,42	0,43	42,65	12,5035
O	34,64	0,63	36,46	77,5077
Si	34,05	0,31	20,42	45,1548
S	0,90	0,39	0,47	2,0077
Total	100,00		100,00	

c.

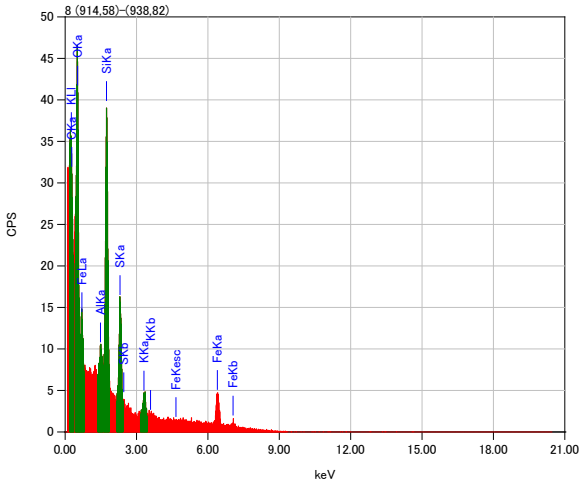

Element	mass%	Error%	At%	K
C	12,20	0,31	23,38	4,8669
O	31,75	0,38	45,68	82,9775
Al	1,22	0,25	1,04	1,2382
Si	11,68	0,25	9,57	13,4312
S	7,18	0,26	5,15	16,4471
K	1,99	0,41	1,17	13,2621
Fe	33,98	2,62	14,01	24,8604
Total	100,00		100,00	

Figure 8 – Energy-dispersive X-ray microanalysis with selected characteristic point measurements of particles of the coarse fraction isolated from the filtration mother liquor concentrate:

(a) particles of the coarse fraction with indicated areas of analysis;

(b) X-ray spectrum of energy-dispersive X-ray microanalysis (point 2);

(c) X-ray spectrum of energy-dispersive X-ray microanalysis (point 8).

Among the sorbent fragments in the coarse fraction, fragments enriched with uranium are also observed; however, the uranium content in such particles does not exceed 5 percent (Figure 9).

The analysis of the precipitates of medium fraction 1 by scanning electron microscopy and energy-dispersive X-ray microanalysis revealed a large number of particles of similar size. The particle size of this fraction lies within a relatively narrow range of 30 to 50 micrometers and represents a mixture of three types of particles composed, respectively, of iron oxides, uranium peroxide, and silicon oxide.

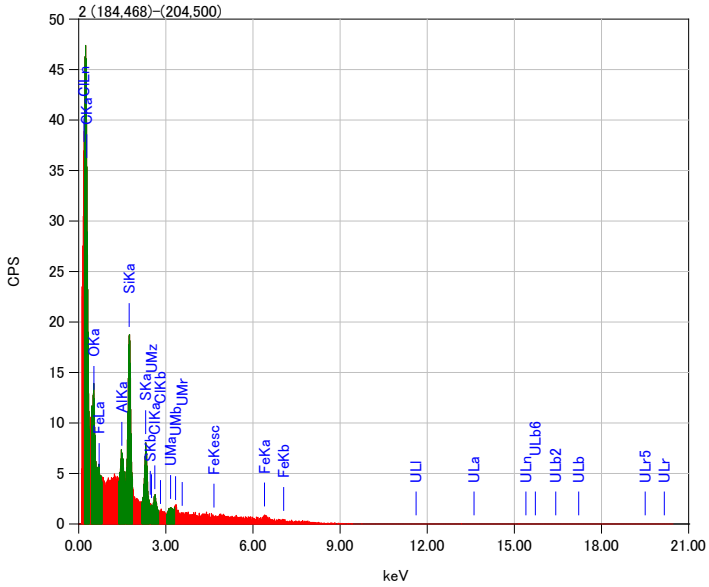

Element	mass%	Error%	At%	K
C	42,02	0,45	60,18	30,6206
O	21,38	1,23	22,98	45,9869
Al	2,02	0,50	1,29	2,6885
Si	12,64	0,53	7,74	18,1063
S	7,40	0,59	3,97	20,0125
Cl	2,12	0,70	1,03	5,0640
Fe	8,10	6,95	2,49	5,9799
U	4,32	3,32	0,31	4,3393
Total	100,00		100,00	

Figure 9 – Representative energy-dispersive X-ray microanalysis spectrum of uranium-containing sorbent fragments

Particles of uranium peroxide constitute approximately one-fifth of medium fraction 1, while three-fifths are composed of iron oxide particles and one-fifth of silicon oxide particles.

Unlike uranium peroxide particles, particles of iron and silicon oxides do not differ visually either in morphology or in color. In contrast, the white particles of the fraction, whose stoichiometric composition corresponds to uranium peroxide, can be visually distinguished. This is due to the fact that, in scanning electron microscopy, image contrast is determined by the atomic number of the elements comprising the analyzed material. When an element is present in a material in a sufficiently compact form as a distinct phase (with a content not less than 0.1 to 0.5 percent by mass within the analyzed volume), and the adjacent phase consists of elements with significantly different atomic numbers, such a phase can be readily identified visually due to atomic number contrast. In scanning electron microscopy images, phases composed of elements with higher atomic numbers appear brighter. Accordingly, in addition to the data obtained by energy-dispersive X-ray microanalysis, all uranium-containing compounds in the precipitates can be readily identified visually in scanning electron microscopy images, appearing as brighter particles against the background of other phases.

a.

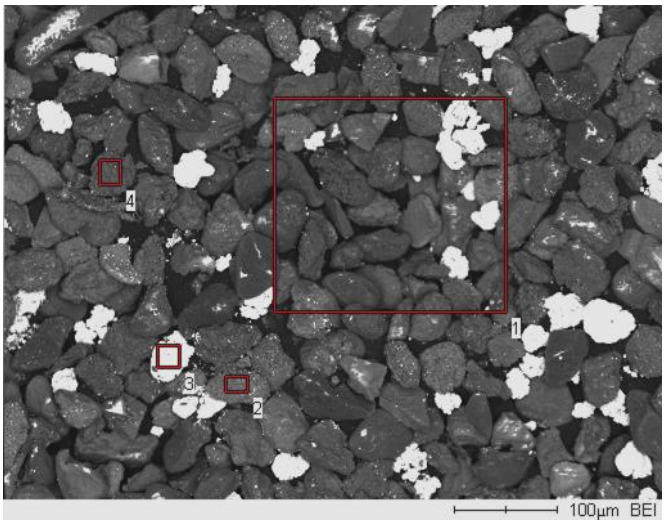

b.

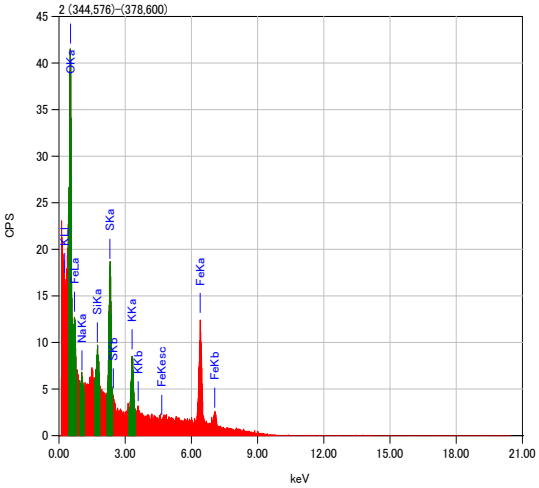

Element	mass%	Error%	At%	K
O	36,03	0,36	61,50	91,7849
Na	1,46	0,49	1,74	2,3646
Si	1,62	0,26	1,57	1,6310
S	11,42	0,26	9,73	24,3965
K	6,06	0,42	4,23	37,2826
Fe	43,41	2,78	21,23	28,1452
Total	100,00		100,00	

c.

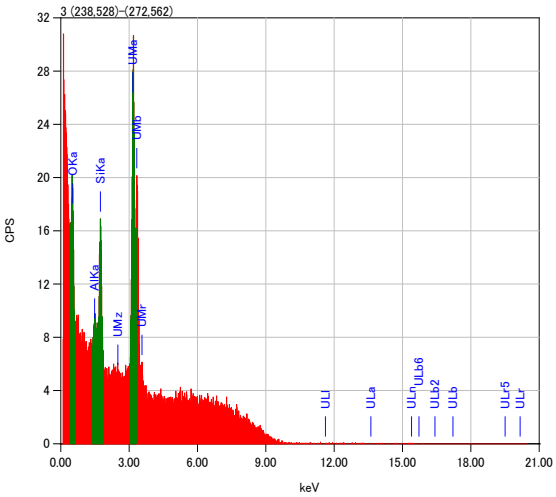

Element	mass%	Error%	At%	K
O K	15,42	0,68	63,47	28,2612
Al K	1,29	0,34	3,16	1,2172
Si K	4,99	0,33	11,71	5,4600
U M	78,29	1,57	21,67	78,2742
Total	100,00		100,00	

Figure 10 – Energy-dispersive X-ray microanalysis of particles of the filtration mother liquor precipitate, medium fraction 1

(a) particles of medium fraction 1 with indicated analysis areas;

(b) X-ray spectrum of energy-dispersive X-ray microanalysis (point 2);

(c) X-ray spectrum of energy-dispersive X-ray microanalysis (point 3).

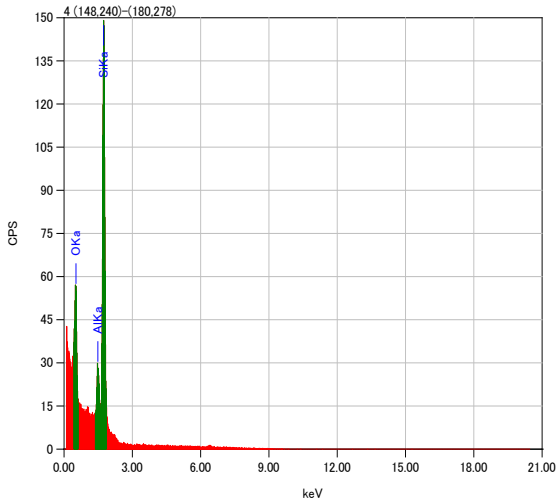

Element	mass%	Error%	At%	K
O	41,69	0,58	55,56	81,0842
Al	6,06	0,30	4,79	5,8070
Si	52,25	0,34	39,66	51,0207
Total	100,00		100,00	

Figure 11 – Energy-dispersive X-ray microanalysis of particles of the filtration mother liquor precipitate, medium fraction 1 (point 4 – Figure 25a)

Analysis of medium fraction 2 based on scanning electron microscopy and energy-dispersive X-ray microanalysis data (Figure 12) shows that the particles of this fraction can be divided into two types: uranium peroxide particles with sizes ranging from 2 to 20 micrometers (not less than 30 percent of the precipitate of this fraction) (Figure 12c), and the remaining portion of the fraction represented by particles of iron oxides, silicates, and aluminosilicates with approximately the same size (Figure 12d).

The averaged energy-dispersive X-ray microanalysis of a precipitate area corresponding to a square with a side length of 150 micrometers (Figure 12b) clearly demonstrates that the uranium content in the precipitate is not less than 40 percent by volume.

Analysis of the fine fraction based on scanning electron microscopy and energy-dispersive X-ray microanalysis data shows that it consists, to a large extent, of fine-dispersed uranium peroxide particles with sizes ranging from 0.1 to 2 micrometers, accounting for approximately 70 to 80 percent of the fraction. The practically complete absence of electrical conductivity of these particles did not allow for a detailed study of their morphology.

Observations by scanning electron microscopy made it possible to conclude that the larger white regions (greater than 2 micrometers) of the fine fraction represent agglomerates of smaller uranium peroxide particles (Figure 13a, 13c).

The darker regions of the fine fraction, as established by observations, also consist of finer particles with sizes less than 1 to 2 micrometers. These particles are predominantly composed of iron oxides and sulfates. The presence of a noticeable amount of carbon in these particles (up to 10 percent) may indicate the presence in this fraction of fine particles of the sorbent material (Figure 13b).

Points 3 and 4 of the energy-dispersive X-ray microanalysis (Figure 13a) have compositions analogous to those of points 2 and 1, respectively; therefore, the corresponding data are not presented in Figure 13.

Thus, the data obtained by scanning electron microscopy and energy-dispersive X-ray microanalysis of the filtration mother liquor concentrate precipitates convincingly confirm the results of the chemical analysis of the precipitate with respect to uranium content (39.2 percent). At the same time, the main portion of uranium in the precipitate is present in the form of uranium peroxide particles ($UO_4 \cdot 2H_2O$) with sizes in the range of 0.1 to 50 micrometers.

a.

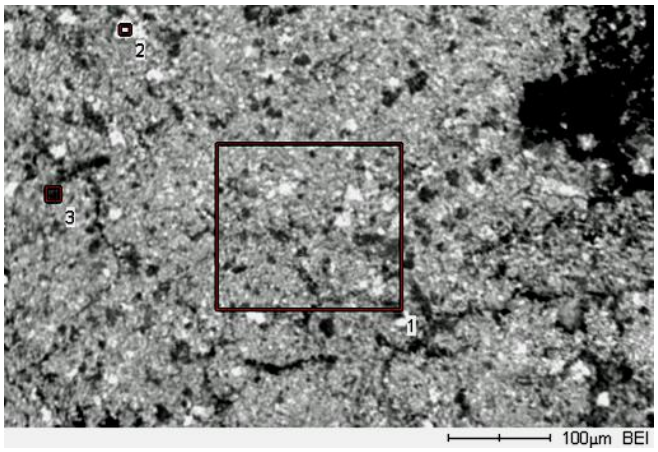

b.

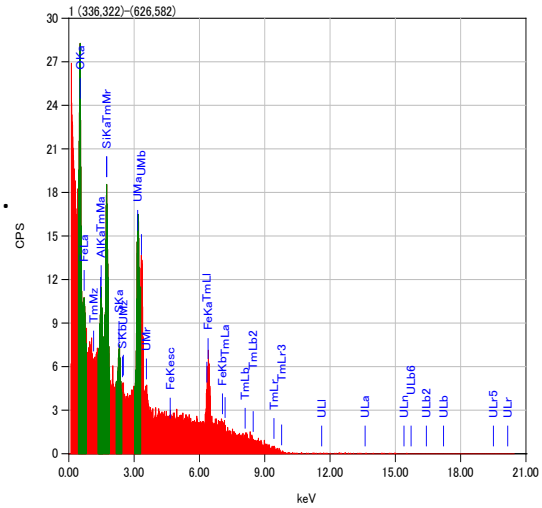

Element	mass%	Error%	At%	K
O	16,92	0,45	62,13	54,1926
Al	1,44	0,75	2,33	1,3791
Si	5,23	0,28	8,10	5,7924
S	2,30	0,27	3,12	5,4190
Fe	19,11	3,10	14,90	12,6552
U	43,19	1,35	7,90	42,5866
Total	100,00		100,00	

c.

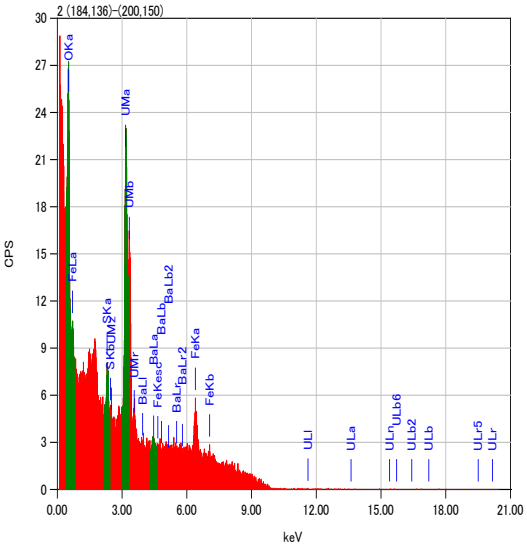

Element	mass%	Error%	At%	K
O	18,39	0,46	65,78	46,9657
S	2,06	0,26	3,31	5,0620
Fe	9,36	3,19	17,89	12,5349
U	70,19	1,31	13,02	57,0041
Total	100,00		100,00	

d.

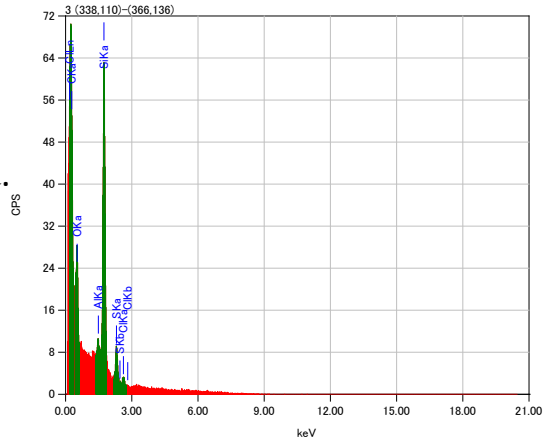

Element	mass%	Error%	At%	K
C	39,99	0,47	53,79	22,6717
O	28,03	1,00	28,30	60,4439
Al	2,71	0,41	1,40	1,6445
Si	24,56	0,44	14,13	35,1695
S	4,71	0,53	2,38	11,8057
Total	100,00		100,00	

Figure 12 – Energy-dispersive X-ray microanalysis of particles of the filtration mother liquor precipitate, medium fraction 2

(a) particles of medium fraction 2 with indicated analysis areas;
(b) X-ray spectrum of energy-dispersive X-ray microanalysis (point 1);
(c) X-ray spectrum of energy-dispersive X-ray microanalysis (point 2);
(d) X-ray spectrum of energy-dispersive X-ray microanalysis (point 3).

a.

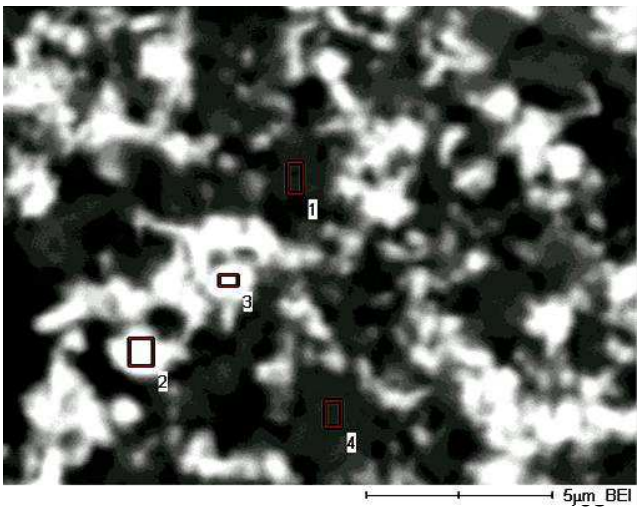

b.

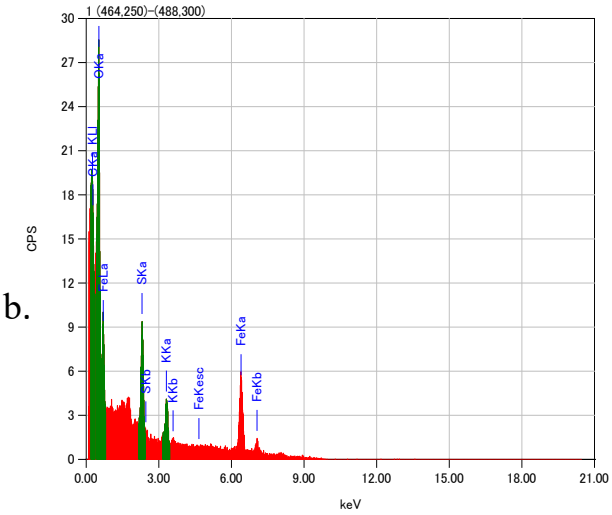

Element	mass%	Error%	At%	K
C	10,01	0,21	20,94	4,9087
O	31,76	0,31	49,89	85,3959
S	6,70	0,22	5,25	15,2319
K	3,79	0,35	2,43	24,9491
Fe	47,74	2,10	21,48	36,5420
Total	100,00		100,00	

c.

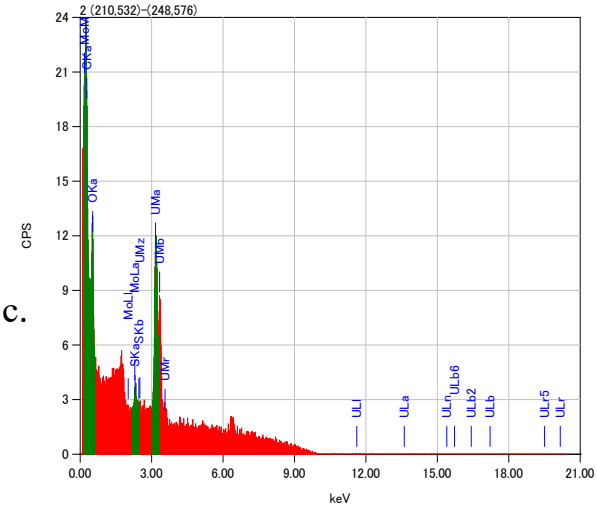

Element	mass%	Error%	At%	K
C	8,93	0,19	29,66	8,9714
O	23,10	0,78	57,58	44,4960
S	1,03	0,74	1,29	2,4602
U	66,94	1,92	11,04	64,9214
Total	100,00		100,00	

Figure 13 – Energy-dispersive X-ray microanalysis of particles of the filtration mother liquor precipitate, fine fraction

(a) particles of the fine fraction with indicated analysis areas;

(b) X-ray spectrum of energy-dispersive X-ray microanalysis (point 1);

(c) X-ray spectrum of energy-dispersive X-ray microanalysis (point 2).

3.3 Analysis of Membrane Fouling, Flux Stability, and Membrane Contamination Mechanisms

One of the key factors determining the industrial applicability of ultrafiltration for the treatment of filtration mother liquors generated during uranium production is membrane fouling, which directly affects flux stability, membrane lifetime, and overall operating costs. [19-22] For membrane-based technologies, analysis of fouling mechanisms is essential, since flux stability determines not only the technological efficiency of the process but also its industrial feasibility.

Preliminary experimental investigations demonstrated that the use of a ceramic ultrafiltration membrane with a pore size of 10 nanometers was accompanied by a sharp decline in permeability, as a result of which filtration was practically terminated after processing approximately 3 dm³ of the feed solution. In contrast, the use of a ceramic membrane with a pore

size of 20 nanometers ensured stable process operation with a specific membrane productivity of approximately 150 $L \cdot m^{-2} \cdot h^{-1}$ and a clarification efficiency of 98.96 percent, indicating a fundamental difference in the fouling mechanisms governing the performance of these membranes.

According to contemporary concepts of membrane processes, flux decline during ultrafiltration can be described within the framework of the Hermia models, which include four principal fouling mechanisms: complete pore blocking, standard blocking, intermediate blocking, and cake filtration. [23, 24] During the initial stages of membrane operation, the decrease in permeability is generally associated with internal or intermediate pore blocking, whereas, with the accumulation of solid material on the membrane surface, the increase in resistance of the surface deposit layer becomes the dominant limiting factor.

Analysis of the experimental results indicates that, for the 10 nanometer membrane, the predominant mechanism was internal pore blocking. This observation is consistent with the results of the morphological analysis of the solid phase, according to which the system contains a fine-dispersed particle fraction with characteristic dimensions of approximately 0.12 micrometers (120 nanometers), accounting for not less than 15 percent of the total precipitate volume, in addition to larger agglomerates. Although the average size of these particles exceeds the nominal pore diameter of the membrane, the colloidal and subcolloidal fractions, as well as irregularly shaped aggregates, are capable of penetrating into the near-surface region of the membrane, thereby forming persistent channel blockage. Under such conditions, a combination of standard blocking and intermediate blocking mechanisms appears to be the most probable, leading to a rapid increase in hydraulic resistance and a practically irreversible decline in flux.

An additional factor governing the intensity of membrane fouling is the chemical composition of the filtration mother liquor. The feed solution is characterized by concentrations of Si of 0.055 g/L, Fe of 0.011 g/L, Al of 0.009 g/L, and SO_4^{2-} of 11.6 g/L, indicating a highly mineralized system and a pronounced potential for inorganic fouling. Silica represents one of the most problematic constituents in membrane processes because of its tendency to form persistent silicate and colloidal structures that give rise to dense and sparingly soluble deposits. Iron-containing compounds, in turn, are prone to the formation of oxide-hydroxide precipitates exhibiting strong adhesion to the membrane surface. The elevated sulfate concentration additionally increases the ionic strength of the medium, resulting in compression of the electrical double layer, reduction of colloidal stability, and accelerated particle aggregation.

The results obtained by scanning electron microscopy and energy-dispersive X-ray microanalysis confirm the presence in the concentrate not only of uranium-bearing particles but also of iron-containing and silicon-containing inclusions, thereby indicating the mixed nature of

membrane contamination. Consequently, fouling in the investigated system involves the simultaneous occurrence of mechanical deposition of the dispersed phase, internal pore blocking, concentration polarization, and chemical inorganic scaling. Such a type of fouling represents one of the most challenging cases from the standpoint of membrane regeneration, since it combines both reversible and irreversible mechanisms of permeability decline.

For quantitative characterization of membrane resistance, the resistance-in-series approach is commonly employed:

$$R_t = R_m + R_r + R_i$$

where:

(R_t) is the total hydraulic resistance of the membrane system;

(R_m) is the resistance of the clean membrane;

(R_r) is the reversible contribution associated with the surface deposit layer (reversible fouling);

(R_i) is the irreversible resistance caused by internal pore blocking and chemical contamination (irreversible fouling).

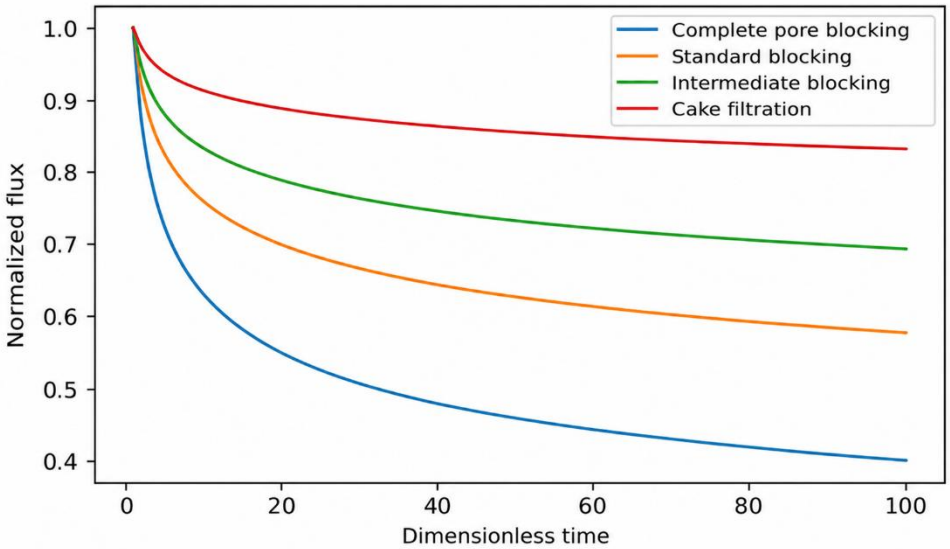

Figure 14 – Conceptual Representation of Fouling Mechanisms According to the Hermia Models

For the theoretical interpretation of the experimentally observed decline in membrane permeability during ultrafiltration of filtration mother liquors, the concept of the classical Hermia models was employed. These models describe the principal mechanisms of membrane fouling occurring during filtration processes. Figure X presents the comparative behavior of the normalized flux as a function of dimensionless time for the four fundamental mechanisms of membrane surface and pore-space contamination.

The graph demonstrates that the most pronounced decline in normalized flux is observed for the complete pore blocking mechanism. In this case, each particle reaching the membrane

surface completely obstructs an individual pore, thereby preventing further liquid transport through the corresponding channel. Such a mechanism is characteristic of systems containing fine-dispersed particles comparable in size to the membrane pore diameter, as well as highly adhesive colloidal particles prone to irreversible fixation at pore entrances. This type of fouling is accompanied by the most rapid and irreversible decline in membrane productivity. In the present investigation, this behavior correlates well with the performance of the 10 nanometer membrane, for which a sharp decrease in flux was observed already at the initial stage of filtration.

The standard blocking mechanism is characterized by a gradual reduction in the effective pore diameter due to the accumulation of foulants on the internal walls of the channels. In contrast to complete blocking, the pores are not instantaneously obstructed; however, their hydraulic resistance continuously increases. The graph shows a pronounced decline in flux, although less abrupt than that observed in the case of complete pore blocking. Such behavior is typical of systems containing fine colloidal particles or dissolved species capable of penetrating into the pore structure and forming internal deposits. In the investigated system, this mechanism may be associated with the penetration of fine-dispersed uranium-bearing phases as well as silicon-containing colloidal structures into the membrane pore space.

Intermediate blocking represents a mixed mechanism in which some particles are deposited directly on the membrane surface, whereas others are deposited on previously accumulated foulants. Under such conditions, not every particle causes blockage of a new pore, and therefore the flux decline occurs more gradually. This regime is characteristic of systems containing moderate concentrations of suspended solids and particles exhibiting a broad size distribution. In the context of the present study, intermediate blocking is most likely associated with the transitional stage between the initial membrane contamination and the subsequent development of a surface deposit layer.

The slowest decline in normalized flux is observed for the cake filtration mechanism. In this case, particles are predominantly deposited on the membrane surface, forming a porous filtration layer that gradually increases the hydraulic resistance of the system. Despite the reduction in flux, this mechanism is considered the most technologically favorable because the contamination is localized primarily on the membrane surface and can generally be removed by hydraulic cleaning or chemical regeneration. Furthermore, the formed deposit layer may function as a secondary dynamic membrane, thereby enhancing the retention efficiency of the fine-dispersed phase. In the investigated system, this mechanism most closely corresponds to the performance of the 20 nanometer membrane, for which stable filtration and a high clarification efficiency of the solution (98.96 percent) were maintained despite the presence of fouling.

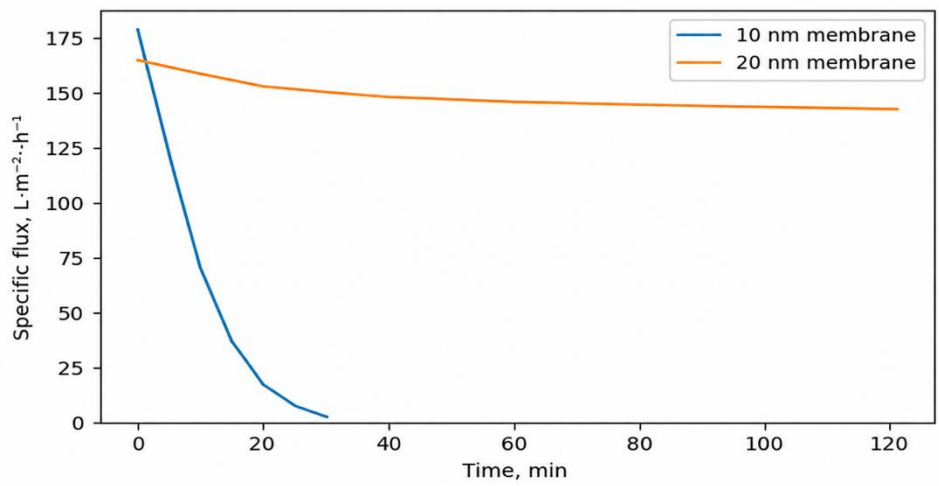

Figure 15 – Comparison of Specific Flux Decline Dynamics for the 10 and 20 Nanometer Membranes

Experimental data describing the variation of specific flux with time make it possible to quantitatively assess the resistance of the membrane system to fouling and to confirm the previously established conclusions regarding the differences in fouling mechanisms for membranes with different pore sizes. As can be seen from the graph presented, the flux decline behavior for the 10 nanometer and 20 nanometer membranes differs fundamentally both in intensity and in the kinetics of fouling development.

For the membrane with a pore size of 10 nanometers, an extremely rapid decline in specific flux is observed. From an initial value of approximately 180 $L \cdot m^{-2} \cdot h^{-1}$, the flux decreases to approximately 70 $L \cdot m^{-2} \cdot h^{-1}$ within the first 10 minutes, corresponding to a reduction exceeding 60 percent. After 15–20 minutes, the flux decreases to approximately 15–35 $L \cdot m^{-2} \cdot h^{-1}$, and by the thirtieth minute it approaches zero. Such a profile indicates a rapid increase in the hydraulic resistance of the system and the effective loss of membrane functionality.

Of particular significance is the fact that the most pronounced decline in flux occurs during the initial stage of filtration. Such behavior is characteristic of systems in which the dominant mechanism is not the gradual accumulation of a surface deposit but rather the rapid blockage of the active filtration structure of the membrane. This indicates that the principal contribution to permeability decline originates from the increase in irreversible resistance ((R_i)), associated with pore blockage and internal contamination of the membrane material. The almost complete cessation of filtration indicates the attainment of a critical state at which further membrane operation without regeneration becomes impossible.

A completely different behavior is observed for the membrane with a pore size of 20 nanometers. In this case, the initial specific flux amounts to approximately 165 $L \cdot m^{-2} \cdot h^{-1}$, followed by a moderate decrease to approximately 150 $L \cdot m^{-2} \cdot h^{-1}$ during the first 20–30 minutes. Subsequent flux reduction proceeds at a significantly slower rate, and even after 120 minutes the flux remains

at a level of approximately 142–145 $L \cdot m^{-2} \cdot h^{-1}$. Consequently, the overall decline in productivity throughout the observation period amounts to only approximately 13–15 percent, indicating substantially greater operational stability of the membrane system.

The flux kinetics observed for the 20 nanometer membrane demonstrate a classical transition toward a quasi-steady-state filtration regime. After a relatively short initial adaptation stage, the rate of flux decline decreases sharply and the curve assumes an almost asymptotic profile. Such behavior indicates the establishment of a dynamic equilibrium between the rate of contaminant transport to the membrane surface and the rate of formation of a stable filtration layer.

From an engineering standpoint, this regime is the most desirable for industrial applications, since it ensures predictable productivity and enables prolonged continuous operation of the membrane unit. Under these conditions, the flux decline is not critical and can be compensated by conventional membrane process management measures.

Comparison of the experimental results with the chemical composition of the filtration mother liquor provides an additional explanation for the observed behavior. The high concentrations of silicon (0.055 g/L), iron (0.011 g/L), and sulfate ions (11.6 g/L) create a system with a pronounced membrane fouling potential. However, the difference in the behavior of the two membranes demonstrates that the determining factor is not solely the solution composition but also the geometrical characteristics of the membrane structure. As the pore diameter decreases, the probability of local blockage of filtration channels increases, whereas enlargement of the pore size shifts the process toward a more stable regime dominated by surface fouling.

An important finding is the relationship between membrane productivity and clarification efficiency. Despite the use of a membrane with a larger pore size, the clarification efficiency of the solution reached 98.96 percent, indicating that high separation efficiency was maintained. This demonstrates that the transition to the 20 nanometer membrane did not result in a critical deterioration of selectivity but substantially improved flux stability. This result is particularly important from the standpoint of industrial implementation, since, in engineering practice, the priority in membrane selection is not the maximum nominal selectivity but rather the stable achievement of the required technological performance over extended periods of operation.

Thus, the experimental specific flux dynamics confirm that the 10 nanometer membrane does not possess sufficient operational stability for the treatment of the investigated filtration mother liquor because of the rapid development of irreversible fouling. In contrast, the 20 nanometer membrane exhibits a stable hydrodynamic regime, limited permeability decline, and high process efficiency, making it the preferred option for further process scale-up and industrial implementation.

The formation of a deposit layer exerts a dual influence on the process. On the one hand, accumulation of the deposit layer leads to an increase in hydraulic resistance and, consequently, to a reduction in permeate flux. On the other hand, once a quasi-steady-state condition has been attained, the formed layer begins to function as a secondary dynamic membrane, thereby enhancing the retention efficiency of fine-dispersed and colloidal particles. This phenomenon explains the combination of a high clarification efficiency (98.96 percent) and satisfactory flux stability observed for the 20 nanometer membrane.

The obtained results are in good agreement with published investigations concerning ultrafiltration of industrial and hydrometallurgical solutions, according to which iron-containing and silica-related fouling represent the principal limiting factors in highly mineralized systems. The literature indicates that, for ceramic membranes, the most favorable operating regime is one in which contamination is localized predominantly on the membrane surface, since this type of fouling can be removed much more efficiently by hydraulic cleaning and chemical regeneration than internal pore blockage.

Thus, the use of a ceramic membrane with a pore size of 20 nanometers represents a technically and technologically justified compromise between separation selectivity and membrane flux stability. Despite the potentially higher selectivity of the 10 nanometer membrane, its application is limited by an excessive tendency toward irreversible pore blockage and rapid growth of the irreversible resistance component, (R_i). In contrast, the 20 nanometer membrane shifts the process into a regime dominated by surface fouling, which is characterized by substantially greater controllability.

For industrial implementation of the technology, the following measures are required:

- optimization of crossflow velocity;
- reduction of local concentration polarization;
- control of the concentrations of Si-, Fe-, and SO_4^{2-}-containing species;
- implementation of hydraulic cleaning procedures;
- application of periodic chemical regeneration using weakly acidic solutions.

From an engineering perspective, such an approach provides the operational stability required for industrial ultrafiltration of filtration mother liquors generated during uranium production.

3.4 Mechanism of Formation of the Ultradisperse Uranium-Bearing Phase in Filtration Mother Liquors

A key aspect in the interpretation of the obtained results is understanding the mechanism of formation of the ultradisperse solid phase in filtration mother liquors, since the

physicochemical nature of these particles determines the efficiency of their recovery by membrane methods, the nature of ceramic ultrafiltration membrane fouling, and the possibility of subsequent uranium recycling into the main process cycle. The presence in the precipitates of compounds such as $UO_4 \cdot 2H_2O$, iron oxyhydroxide species, and silicon-containing silicate phases indicates a complex multistage mechanism of formation of the dispersed solid system, involving chemical precipitation, nucleation, crystal growth, aggregation, and subsequent partial disaggregation.

3.4.1 Chemical Nature of Uranium-Bearing Solid Phase Formation.

The formation of uranium-bearing particles in the investigated process system is directly associated with peroxide precipitation of uranium. In acidic sulfate process solutions, uranium(VI) exists predominantly in the form of uranyl ions and their stable sulfate complexes. At elevated sulfate concentrations, the principal uranium species are $[UO_2(SO_4)_2]^{2-}$ and $[UO_2(SO_4)_3]^{4-}$. These complexes possess high thermodynamic stability, which ensures the preservation of uranium in dissolved form under acidic process conditions.

Upon the addition of hydrogen peroxide, interaction with uranyl ions occurs, resulting in the formation of intermediate peroxo-complex compounds, which, upon reaching a critical supersaturation level, transform into a sparingly soluble solid phase:

$$UO_2^{2+}+H_2O_2+2H_2O \rightarrow UO_4 \cdot 2H_2O\downarrow+2H^+$$

This process represents a chemical precipitation reaction controlled by the degree of supersaturation of the solution.

Unlike slow equilibrium crystallization processes, peroxide precipitation is characterized by high kinetic intensity, as a result of which the system rapidly reaches a state of local supersaturation.

Nucleation mechanism.

The formation of the solid phase begins with the generation of primary crystallization centers.

The nucleation rate is determined by the following relationship:

$J_n \propto \exp(-\Delta G^*/kT)$, where:

J_n is the nucleation rate;

ΔG^* is the energy barrier for the formation of a critical nucleus;

k is the Boltzmann constant;

T is the absolute temperature.

The degree of supersaturation is defined as:

$S=C/Ceq$, where:

C is the current concentration of the dissolved substance;

Ceq is the equilibrium solubility.

As the degree of supersaturation increases, the energy barrier for nucleation decreases, whereas the rate of formation of crystallization centers increases exponentially.

Under peroxide precipitation conditions, the high rate of chemical interaction results in the virtually instantaneous formation of a large number of crystallization centers. Under these conditions, the nucleation rate becomes substantially greater than the growth rate of individual crystals.

This corresponds to the following kinetic regime: nucleation> crystal growth.

It is precisely this mechanism that constitutes the fundamental cause of the formation of the ultradisperse solid phase, since, instead of a limited number of large crystals, a considerable number of fine-dispersed particles are formed.

3.4.2 Heterogeneous nucleation

In a real process system, the process proceeds predominantly via heterogeneous nucleation rather than through the idealized homogeneous formation of crystalline nuclei.

This is due to the presence in process solutions of:

- iron hydroxide compounds;
- silicon-containing colloidal particles;
- mechanical impurities;
- residual microparticles of the solid phase.

These components act as energetically favorable crystallization centers, since they significantly reduce the energy barrier for the formation of a new phase. The role of iron-containing compounds is particularly important. Iron oxyhydroxide compounds possess:

- high specific surface area;
- developed surface reactivity;
- pronounced sorption capacity toward uranyl ions.

As a result, iron-containing particles become effective centers for uranium precipitation, which explains the presence of mixed iron-uranium aggregates in the investigated precipitate.

3.4.3 Role of medium acidity

The acidity of the process medium exerts a decisive influence on the stability of uranium-bearing complexes.

In a sulfuric acid system, the stability of uranium in dissolved form is determined by:

- the concentration of free sulfuric acid;
- the sulfate ion concentration;

- the local pH value;
- temperature.

Even when the overall acidic conditions of the solution are maintained, microzones with different chemical conditions may arise locally, particularly in the vicinity of the reagent addition point. Within these microzones, the following processes occur:

- ocal decomposition of stable sulfate complexes;
- reduction in uranium solubility;
- a sharp increase in the degree of supersaturation;
- initiation of precipitation.

Thus, the acidity of the medium exerts a direct influence not only on the thermodynamic stability of complex species but also on the kinetics of dispersed phase formation.

3.4.4 Role of Peroxide Precipitation in the Formation of Ultradisperse Particles

A principal feature of peroxide precipitation is the high chemical reaction rate. Unlike slower precipitation processes dominated by gradual crystal growth, this process exhibits intensive mass formation of nucleation centers. Consequently, nucleation dominates over particle growth.

Insufficient mixing amplifies this effect, as zones of extremely high local supersaturation develop near the point of hydrogen peroxide addition. As a result, a stable ultradisperse uranium-bearing phase is generated.

The sulfate medium exerts a dual influence. On one hand, sulfate ions stabilize uranium in dissolved form through complexation. On the other hand, the high ionic strength compresses the electrical double layer, reduces the electrostatic stability of particles, and promotes aggregation. Therefore, in sulfate process solutions, dissolved uranyl-sulfate complexes and ultradisperse uranium-bearing solid phases can coexist.

The presence of iron-containing and silicon-containing phases further promotes the formation of the ultradisperse system. Iron oxyhydroxides act as centers for heterogeneous nucleation and sorb uranyl ions on their surfaces. Silicon-containing colloids stabilize the fine-dispersed phase, preventing particle coarsening. The detection of $UO_4 \cdot 2H_2O$, iron oxides, and silicates in the precipitate indicates a combined mechanism: uranium peroxide precipitation, heterogeneous nucleation, and colloidal stabilization. After the formation of primary particles, the system reaches a dynamic equilibrium between aggregation and disaggregation. High mineralization and the presence of Fe/Si components favor aggregation, whereas mixing and shear stresses induce disaggregation. This maintains a broad particle size distribution in filtration mother liquors, including a persistent ultradisperse fraction.

Thus, the formation of the ultradisperse uranium-bearing phase results from the combined effects of: high kinetic intensity of peroxide precipitation, local supersaturation, heterogeneous nucleation on Fe/Si-containing particles, pH influence, complexation in the sulfate medium, dynamic equilibrium between aggregation and disaggregation.

This mechanism explains why such particles are poorly removed by conventional filter-press filtration but can be efficiently concentrated and retained using ceramic ultrafiltration.

4. Conclusions

This research demonstrates that ceramic ultrafiltration is a scientifically justified and technologically effective method for reducing irrecoverable uranium losses associated with ultradisperse and colloidal particles formed after peroxide precipitation. The combination of SEM, EDS and membrane filtration established the morphology, composition and origin of uranium-bearing particles responsible for process losses. Conventional filtration was shown to be insufficient because most uranium losses are associated with particles smaller than 1 μm. Experimental studies confirmed that a 20 nm ceramic membrane achieved up to 98.96% clarification while concentrating uranium to 39.2% in the recovered solid phase. The results prove that ultrafiltration enables selective concentration and return of the dispersed uranium-bearing phase to the production cycle. Compared with ion exchange, thickening, centrifugation, nanofiltration and reverse osmosis, ultrafiltration most closely matches the separation objective because it targets the dispersed phase rather than dissolved uranium. The proposed approach has high industrial relevance owing to its modularity, compatibility with existing flowsheets, relatively low operating costs, expected payback of approximately 1–3 years and potential recovery of a significant proportion of uranium previously lost with mother liquors. Overall, the study provides both scientific justification and practical guidance for industrial implementation of ceramic ultrafiltration and establishes a foundation for further optimization of membrane materials, pore size, regeneration protocols and long-term operating conditions.

Acknowledgements

This research was funded by the Committee of Science of the Ministry of Science and Higher Education of the Republic of Kazakhstan (Grant No. BR28713471) entitled “Development of methods for increasing the extraction of uranium from uranium-containing solutions by effectively reducing the content of silicon compounds”.

Competing interests

The authors declare no competing interests.

Data availability statement

The datasets used and/or analysed during the current study available from the corresponding author on reasonable request.

References

[1] Kalintsev A. et al. Nature and coordination geometry of geologically relevant aqueous Uranium(VI) complexes up to 400 ºC: A review and new data. Journal of Hazardous Materials. 2023. https://doi.org/10.1016/j.jhazmat.2023.131309

[2] Grambow B. et al. Solids, colloids, and the hydrolysis of tetravalent uranium in chloride media. Frontiers in Nuclear Engineering. 2023. https://doi.org/10.3389/fnuen.2023.1308064

[3] International Atomic Energy Agency. Uranium Extraction Technology. Technical Reports Series No. 359. Vienna: International Atomic Energy Agency, 1993. URL: https://www-pub.iaea.org/MTCD/Publications/PDF/trs359_web.pdf

[4] International Atomic Energy Agency. Technologies for the Treatment of Effluents from Uranium Mines, Mills and Tailings. IAEA-TECDOC-1296. Vienna: International Atomic Energy Agency, 2002. URL: https://www-pub.iaea.org/MTCD/publications/PDF/te_1296_prn%5Ct1296_part1.pdf

[5] Gandhi T. P. et al. A critical review of uranium contamination in groundwater: Treatment and sludge disposal. Science of the Total Environment. 2022. https://doi.org/10.1016/j.scitotenv.2022.153947

[6] He Z., et al. *Nano-scale Analysis of Uranium Release Behavior From River Sediment in the Ili Basin.* Water Research. 2022, 227, 119321. https://doi.org/10.1016/j.watres.2022.119321

[7] Tanudjaja H. J. et al. A review of membrane fouling by proteins in ultrafiltration and microfiltration. Journal of Water Process Engineering. 2022. https://doi.org/10.1016/j.jwpe.2022.103294

[8] Maria E., Faucher S., Crançon P., Lespes G. *Centrifugal ultrafiltration preconcentration for studying the colloidal phase of a uranium-containing soil suspension.* Journal of Chromatography A. 2021. https://doi.org/10.1016/j.chroma.2021.461957

[9] Kammakakam I. Next-generation ultrafiltration membranes: A review of material design, properties, recent progress, and challenges. Chemosphere. 2023. https://doi.org/10.1016/j.chemosphere.2022.137669

[10] Staszak K., Wieszczycka K. *Recovery of Metals from Wastewater—State-of-the-Art Solutions with the Support of Membrane Technology*. Membranes. 2023. https://doi.org/10.3390/membranes13010114

[11] Algieri C. et al. *A Way to Membrane-Based Environmental Remediation for Heavy Metal Removal*. Environments. 2021. https://doi.org/10.3390/environments8060052

[12] Han S. et al. *Earth System Science Applications of Next-Generation SEM-EDS Automated Mineral Mapping*. Frontiers in Earth Science. 2022. https://doi.org/10.3389/feart.2022.956912

[13] Xing C. et al. Application of Ultra/Nanofiltration Membrane in Uranium Rejection from Fresh and Salt Waters. Separation and Purification Technology. 2023. https://doi.org/10.1016/j.seppur.2023.123543

[14] Raff O., Wilken R.-D. Uranium Removal from Water by Nanofiltration. In: Proceedings of the International Mine Water Association Symposium. 1999. https://imwa.info/docs/imwa_1999/IMWA1999_Raff_321.pdf

[15] Favre-Reguillon A. et al. Selective removal of dissolved uranium in drinking water by nanofiltration. Water Research. 2008. https://doi.org/10.1016/j.watres.2007.08.034

[16] Ma H. et al. Radioactive Wastewater Treatment Technologies: A Review. Molecules. 2023. https://doi.org/10.3390/molecules28041935

[17] Yazzie C. B., Elias C., Karanikola V. Uranium rejection with nanofiltration membranes and the influence of environmentally relevant mono- and divalent cations at various pH. Environmental Science: Water Research and Technology. 2024. https://doi.org/10.1039/d4ew00324a

[18] Wu S., Ma B., Fan H. et al. Influence of water quality factors on cake layer 3D structures and water channels during ultrafiltration process. Water Research. 2023. Vol. 242. 120226. https://doi.org/10.1016/j.watres.2023.120226

[19] Gruskevica K., Mezule L. *Cleaning Methods for Ceramic Ultrafiltration Membranes Affected by Organic Fouling*. Membranes, 2021, 11(2), 131. https://doi.org/10.3390/membranes11020131

[20] Li B., Wang R., Zuo W. et al. *Development of Fouling-Control Strategy for Ceramic Membrane Bioreactor Applied in Partial Nitrification Process*. Water, 2023, 15(3), 444. https://doi.org/10.3390/w15030444

[21] Lv Z., Zhang S., Jiao W. et al. *High-efficiency Cleaning Technology and Lifespan Prediction for the Ceramic Membrane Treating Secondary Treated Effluent*. Water Science and Technology, 2023, 88(1), 321–338. https://doi.org/10.2166/wst.2023.209

[22] *Lin B. et al. Adsorption and Cake Layer Fouling in Relation to Fenton Cleaning of Ceramic Nanofiltration Membranes*. Journal of Membrane Science, 2023, 687, 122097. https://doi.org/10.1016/j.memsci.2023.122097

[23] Pereira G.L.D., Cardozo-Filho L., Jegatheesan V., Guirardello R. *Generalization and Expansion of the Hermia Model for a Better Understanding of Membrane Fouling*. Membranes, 2023, 13(3), 290. https://doi.org/10.3390/membranes13030290

[24] Shams H. et al. *Fouling mechanisms in anoxic-aerobic sequencing batch membrane bioreactor based on adapted Hermia models and main foulant characteristics*. Journal of Environmental Management, 2022, 323, 116146. https://doi.org/10.1016/j.jenvman.2022.116146